

Novel Oligodipyridylamine Ligands with Chiral *N*-Alkyl Side Chains. Synthesis of Coordination Polymers Consisting of Copper Complexes Containing the Ligands and Their Crystal Structure and Optical and Magnetic Properties

Isao Yamaguchi, Emiko Fujinaga, Tomoji Ozeki,[1] and Takakazu Yamamoto*

Chemical Resources Laboratory, Tokyo Institute of Technology, 4259 Nagatsuta, Midori-ku, Yokohama 226-8503

[1]Department of Chemistry and Materials Science, Tokyo Institute of Technology, 2-12-1 O-okayama, Meguro-ku, Tokyo 152-8551

Received March 3, 2004; E-mail: tyamamot@res.titech.ac.jp

Dipyridylamine (dpa) oligomers having chiral (*S*)-2-methylbutyl (MB) side chains at the amine-N atoms, **(MBdpa)$_m$** (H–(C_5H_3N–N(MB)–C_5H_3N)$_m$–H; $m = 2$, 3, and 4), were synthesized. Complexation of **(MBdpa)$_2$** with $CuCl_2$ provided a coordination polymer, **[{Cu$_2$Cl$_4$–(MBdpa)$_2$}$_n$]**. Single-crystal X-ray analysis of **[{Cu$_2$Cl$_4$–(MBdpa)$_2$}$_n$]** showed that intermolecular interactions linked the **Cu$_2$Cl$_4$–(MBdpa)$_2$** complexes into one-dimensional coordination polymers. The crystal of **[{Cu$_2$Cl$_4$–(MBdpa)$_2$}$_n$]** exhibited a phase transition between 100 and 85 K due to the ordering of the MB side chains, resulting in a quadrupling of the unit cell. **(MBdpa)$_m$** had an expanded electron system along the oligomer main chain as revealed by UV–vis spectroscopy. **(MBdpa)$_m$** were photoluminescent in solutions and copper complexation quenched their photoluminescence.

Coordination polymers based on transition metal atoms and organic ligands are the subject of increasing interest due to their unique crystal structures.[1–17] Metal complexation of dimeric aromatic ligands is one of the convenient methods for construction of the coordination polymer.[15,16]

For construction of such a coordination polymer in this work, we selected a derivative of 2,2′-dipyridylamine (dpa) as a starting material. Metal complexes containing dpa have been attracting much attention due to their unique crystal structures.[18–32] Recently, *N*-alkylation of dpa has been reported to give an ligand (Rdpa) useful for functional metal complexes.[32] In this work, we designed a new ligand for coordination polymer: a dimer of dpa with chiral (*S*)-2-methylbutyl (MB) side chains at the amine-N atoms, **(MBdpa)$_2$** (Chart 1). A coordination polymer was obtained by using a reaction of **(MBdpa)$_2$** with copper(II) chloride. X-ray crystallographic analysis revealed that the coordination polymer caused a phase transition at low temperature, which altered the lattice unit volume.

On the other hand, it has been reported that derivatives of dpa show interesting optical properties such as emission of blue light.[33–35] In order to expand the scope of the chemistry of dpa, we also prepared longer oligomeric ligands, **(MBdpa)$_3$** and **(MBdpa)$_4$** (Chart 2), and investigated their optical properties.

Here we report results obtained about **(MBdpa)$_m$** ($m = 2$, 3, and 4) and the coordination polymer of **(MBdpa)$_2$** with Cu(II).

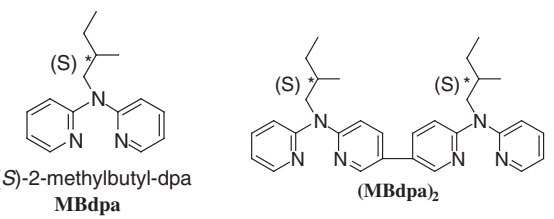

Chart 1.

Experimental

Synthesis of MBdpa. A DMSO solution (20 mL) of NaH (0.20 g, 8.4 mmol) was stirred at 40 °C for 0.5 h and at 75 °C for 1 h. To the solution was added 2,2′-dipyridylamine, dpa, (1.20 g, 7.0 mmol). After stirring at 60 °C for 12 h, (*S*)-2-methylbutyliodide (1.6 mL, 7.3 mmol) was added, and the solution was stirred at 60 °C for 24 h. To the reaction mixture was added water, and the product was extracted with ether. After the organic layer

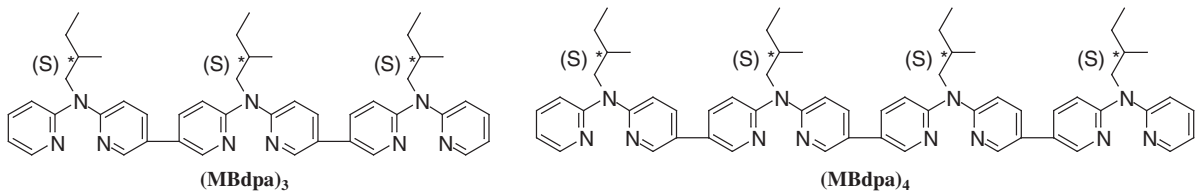

Chart 2.

Published on the web September 10, 2004; DOI 10.1246/bcsj.77.1773

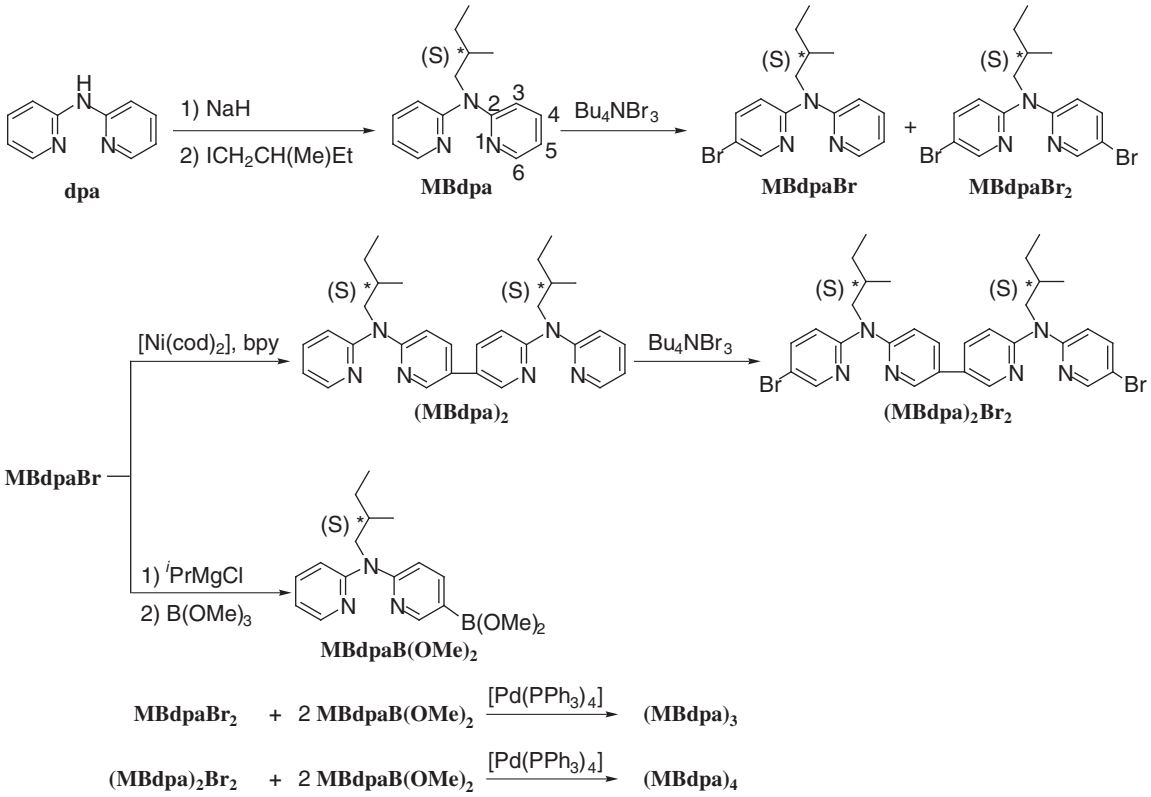

Scheme 1.

was dried over Na_2SO_4, the solvent was removed by evaporation to give a yellow liquid, which was purified by silica gel column chromatography (eluent = $CHCl_3$). The solvent was removed by evaporation and the resulting liquid was dried in vacuo to give **MBdpa** (py–N(MB)–py; py = 2-pyridyl) as a yellow liquid (0.57 g, 34%). ^{1}H NMR (400 MHz, $CDCl_3$, 25 °C) δ 8.32 (dd, 2H, 6-H of py, $J = 2.0$ and 4.8 Hz), 7.50 (td, 2H, 4-H of py, $J = 3.6$ and 8.8 Hz), 7.07 (d, 2H, 5-H of py, $J = 8.8$ Hz), 6.83 (td, 2H, 3-H of py, $J = 3.6$ and 4.8 Hz), 4.07 (m, 2H, NCH_2), 1.89 (m, 1H, C*H*(Me)), 1.49 and 1.14 (m, 2H, CH(Me)CH_2), 0.88 (m, 6H, Me).

Synthesis of MBdpaBr and MBdpaBr$_2$. (cf. Scheme 1). To a chloroform solution (20 mL) of Bu_4NBr_3 (2.2 g, 4.6 mmol; Bu = butyl) was added dropwise a chloroform solution (15 mL) of **MBdpa** (0.70 g, 3.1 mmol), and the mixture was stirred at 20 °C for 12 h. After an aqueous solution of sodium thiosulfate was added to the reaction mixture, the organic layer was separated and dried over Na_2SO_4. The solvent was removed by evaporation and the resulting yellow liquid was purified by silica gel column chromatography (eluent = $CHCl_3$) to give **MBdpaBr** (R_f = 0.14, 0.33 g, 34%) and **MBdpaBr$_2$** (R_f = 0.46, 0.53 g, 43%) as yellow liquids.

Data of MBdpaBr: ^{1}H NMR (400 MHz, $CDCl_3$, 25 °C) δ 8.34 (dd, 1H, 6-H of py, $J = 1.6$ and 4.8 Hz), 8.31 (d, 1H, 6-H of pyBr, $J = 2.8$ Hz), 7.56 (td, 1H, 4-H of py, $J = 3.6$ and 8.4 Hz), 7.54 (dd, 1H, 4-H of pyBr, $J = 2.8$ and 8.8 Hz), 7.10 (d, 1H, 3-H of py, $J = 8.4$ Hz), 6.97 (d, 1H, 3-H of pyBr, $J = 8.8$ Hz), 6.90 (td, 1H, 5-H of py, $J = 3.6$ and 4.8 Hz), 4.02 (m, 2H, NCH_2), 1.86 (m, 1H, C*H*(Me)), 1.45 and 1.13 (m, 2H, CH(Me)CH_2), 0.87 (m, 6H, Me). Anal. Calcd for $C_{15}H_{18}N_3Br$: C, 56.26; H, 5.67; N, 13.12; Br, 24.95%. Found: C, 56.46; H, 5.94; N, 12.84; Br, 25.14%.

Data of MBdpaBr$_2$: ^{1}H NMR (400 MHz, $CDCl_3$, 25 °C) δ 8.33 (d, 2H, 6-H of pyBr, $J = 2.4$ Hz), 7.60 (dd, 2H, 4-H of pyBr, $J = 2.4$ and 8.8 Hz), 7.00 (d, 2H, 3-H of pyBr, $J = 8.8$ Hz), 3.99 (m, 2H, NCH_2), 1.85 (m, 1H, C*H*(Me)), 1.45 and 1.13 (m, 2H, CH(Me)CH_2), 0.87 (m, 6H, Me). Anal. Calcd for $C_{15}H_{17}N_3Br_2$: C, 45.14; H, 4.29; N, 10.53; Br, 40.04%. Found: C, 45.03; H, 4.30; N, 10.49; Br, 40.43%.

Synthesis of (MBdpa)$_2$. To a DMF solution (15 mL) of bis(1,5-cyclooctadiene)nickel(0),[36] [Ni(cod)$_2$], (0.85 g, 3.1 mmol), 2,2′-bipyridyl, bpy, (0.48 g, 3.1 mmol), and cod (0.34 g, 3.1 mmol), was added **MBdpaBr** (0.50 g, 1.6 mmol). After the reaction mixture was stirred at 60 °C for 48 h, the solvent was removed by evaporation, and the product was extracted with chloroform. The extract was washed with brine. The organic layer was dried over sodium sulfate and the solvent was removed by evaporation to give a yellow liquid. Purification by silica gel column chromatography (eluent = ethyl acetate/hexane (v/v = 3/1)) gave **(MBdpa)$_2$** (py–N(MB)–py′–py′–N(MB)–py; py = 2-pyridyl; py′ = pyridine-2,5- or -5,2-diyl) as a yellow liquid (0.28 g, 75%). ^{1}H NMR (400 MHz, $CDCl_3$, 25 °C) δ 8.53 (d, 2H, 6-H of py′, J = 2.4 Hz), 8.35 (dd, 2H, 6-H of py, $J = 2.0$ and 4.8 Hz), 7.68 (dd, 2H, 4-H of py′, $J = 6.8$ and 8.8 Hz), 7.56 (td, 2H, 4-H of py, J = 8.7 and 8.8 Hz), 7.15 (d, 4H, 3-H of py and 3H-py′, $J = 8.8$ Hz), 6.85 (t, 2H, 5-H of py, $J = 6.8$ Hz), 4.12 (m, 4H, NCH_2), 1.93 (m, 2H, C*H*(Me)), 1.50 and 1.15 (m, 4H, CH(Me)CH_2), 0.89 (m, 12H, Me). ^{13}C NMR (100 MHz, $CDCl_3$, 25 °C) δ 157.8, 157.0, 148.3, 145.6, 137.1, 134.7, 126.4, 117.2, 115.4, 114.4, 54.0, 34.0, 27.1, 16.9, 11.4. Anal. Calcd for $C_{30}H_{36}N_6$: C, 74.97; H, 7.55; N, 17.48%. Found: C, 74.91; H, 7.55; N, 17.20%.

Synthesis of (MBdpa)$_2$Br$_2$. To a chloroform solution (5 mL) of Bu_4NBr_3 (0.24 g, 0.50 mmol) was added dropwise a chloroform solution (4 mL) of **(MBdpa)$_2$** (0.16 g, 0.33 mmol), and

the mixture was stirred at 20 °C for 12 h. After an aqueous solution of sodium thiosulfate was added to the reaction mixture, the organic layer was separated and dried over Na_2SO_4. The solvent was removed by evaporation and a resulting yellow liquid was purified by silica gel column chromatography (eluent = ethyl acetate/hexane (v/v = 1/3)) and by HPLC (eluent = chloroform) to give **(MBdpa)Br$_2$** (0.15 g, 69%) as a yellow liquid. ^{1}H NMR (400 MHz, $CDCl_3$, 25 °C) δ 8.53 (d, 2H, 6-H of py′, J = 2.8 Hz), 8.35 (d, 2H, 6-H of pyBr, J = 3.2 Hz), 7.73 (dd, 2H, 4-H of py′, J = 2.4 and 8.8 Hz), 7.61 (dd, 2H, 4-H of pyBr, J = 2.4 and 8.8 Hz), 7.18 (d, 2H, 3-H of py′, J = 8.4 Hz), 7.06 (d, 2H, 3-H of pyBr, J = 8.8 Hz), 4.08 (m, 4H, NCH_2), 1.92 (m, 2H, C*H*(Me)), 1.48 and 1.16 (m, 4H, CH(Me)CH_2), 0.89 (m, 12H, Me). Anal. Calcd for $C_{30}H_{34}N_6Br_2$: C, 56.44; H, 5.37; N, 13.12; Br, 23.99%. Found: C, 57.80; H, 6.15; N, 12.53; Br, 23.99%. MS (FAB) m/z 639 ([M + H$^+$]).

Synthesis of (MBdpa)$_3$ and (MBdpa)$_4$. To a THF solution (5 mL) of **MBdpaBr** (0.43 g, 1.3 mmol) was added dropwise a THF solution of ^{i}PrMgCl (2 M, 1.3 mL) at 0 °C. After the reaction mixture was stirred at 0 °C for 20 h, trimethyl borate (0.69 mL, 6.7 mmol) was added at −78 °C and the reaction mixture was stirred at −78 °C for 2 h and at 20 °C for 24 h under nitrogen atmosphere. To the reaction mixture was added water (100 mL), and the product was extracted with chloroform. After the organic layer was dried over sodium sulfate, the solvent was removed by evaporation to give 5-bis(methoxy)borylpyridine-2-yl-(*S*)-2-methylbutyl-(pyridine-2-yl)amine, **MBdpaB(OMe)$_2$**, as a light brown solid. **MBdpaB(OMe)$_2$** was used for the further reaction without purification. To a THF solution (5 mL) of **MBdpaBr$_2$** (0.34 g, 0.85 mmol) and **MBdpaB(OMe)$_2$** (1.7 g, 2.1 mmol) were added [Pd(PPh$_3$)$_4$] (0.24 g, 0.21 mmol) and an aqueous solution (12 mL) of sodium carbonate (1.2 g, 1.1 mmol). After stirring at 60 °C for 48 h, the reaction product was extracted with chloroform. The organic layer was dried over sodium sulfate and evaporation of the solvent gave a yellow liquid, which was purified by silica gel column chromatography (eluent = ethyl acetate/hexane (v/v = 3/1)) and by HPLC (eluent = chloroform). The solvent was removed by evaporation to give **(MBdpa)$_3$** (py–N(MB)–py′–py″–N(MB)–py″–py′–N(MB)–py; py = 2-pyridyl; py′ and py″ = pyridine-2,5- or -5,2-diyl) as a yellow liquid (60 mg, 15%). ^{1}H NMR (500 MHz, $CDCl_3$, 25 °C) δ 8.55 (dd, 4H, 6-H of py″ and 6-H of py′, J = 2.3 and 2.8 Hz), 8.36 (dd, 2H, 6-H of py, J = 1.3 and 5.0 Hz), 7.72 (dd, 2H, 4-H of py″, J = 2.7 and 8.7 Hz), 7.70 (dd, 2H, 4-H of py′, J = 2.3 and 8.7 Hz), 7.56 (td, 2H, 4-H of py, J = 1.4, 6.9, and 8.7 Hz), 7.21 (d, 2H, 3-H of py″, J = 8.7 Hz), 7.16 (d, 4H, 3-H of py″ and 3-H of py, J = 8.7 Hz), 6.89 (d, 2H, 5-H of py, J = 5.0 and 6.9 Hz), 4.13 (m, 6H, NCH_2), 1.95 (m, 3H, C*H*(Me)), 1.52 and 1.18 (m, 6H, CH(Me)CH_2), 0.91 (m, 18H, Me). ^{13}C NMR (125 MHz, $CDCl_3$, 25 °C) δ 157.8, 157.1, 156.8, 148.3, 145.7, 145.6, 137.2, 134.9, 134.8, 126.9, 126.3, 117.3, 115.5, 114.9, 114.4, 54.1, 54.0, 34.1, 27.2, 27.1, 17.0, 11.5, 11.4. Anal. Calcd for $C_{45}H_{53}N_9$: C, 75.07; H, 7.42; N, 17.51%. Found: C, 74.33; H, 7.42; N, 17.51%. MS (FAB) m/z 721 ([M + H$^+$]).

Synthesis of (MBdpa)$_4$. (py–N(MB)–py′–py″–N(MB)–py‴–py‴–N(MB)–py″–py′–(MB)–py; py = 2-pyridyl; py′, py″, and py‴ = pyridine-2,5- or -5,2-diyl) was synthesized by reaction of **(MBdpa)$_2$Br$_2$** with **MBdpaB(OMe)$_2$** in a similar manner. ^{1}H NMR (500 MHz, $CDCl_3$, 25 °C) δ 8.55 (dd, 6H, 6-H of py′, 6-H of py″, and 6-H of py‴, J = 2.3 and 2.8 Hz), 8.36 (d, 2H, 6-H of py, J = 2.3 Hz), 7.73 (dd, 4H, 4-H of py″ and 4-H of py′, J = 2.8 and 8.7 Hz), 7.70 (dd, 2H, 4-H of py‴, J = 2.3 and 8.7 Hz), 7.56 (td, 2H, 4-H of py, J = 2.3 and 8.3 Hz), 7.23 (d, 4H, 3-H of py′ and 3-H of py″, J = 8.7 Hz), 7.16 (d, 4H, 3-H of py and 3-H of py‴, J = 8.3 Hz), 6.89 (td, 2H, 5-H of py, J = 4.1 and 7.4 Hz), 4.15 (m, 8H, NCH_2), 1.96 (m, 4H, C*H*(Me)), 1.53 and 1.18 (m, 8H, CH(Me)CH_2), 0.89 (m, 24H, Me). ^{13}C NMR (125 MHz, $CDCl_3$, 25 °C) δ 157.8, 157.1, 156.9, 156.8, 148.4, 145.7, 145.6, 137.2, 135.0, 134.8, 127.0, 126.7, 126.3, 117.3, 115.5, 114.9, 114.4, 54.1, 54.0, 34.1, 27.2, 27.1, 17.0, 11.4. MS (FAB) m/z 960 ([M + H$^+$]).

Synthesis of [{Cu$_2$Cl$_4$–(MBdpa)$_2$}$_n$]. A methanol solution (0.5 mL) of $CuCl_2$ (2.65 mg, 0.02 mmol) was placed on a methanol solution (0.5 mL) of **(MBdpa)$_2$** (4.8 mg, 0.010 mmol) in an NMR sample tube (radius = 5 mm). Mixing of the two solutions was carefully avoided. Standing the two-layer solution at room temperature for 7 days gave green crystals (1.6 mg, 21%) of **[{Cu$_2$Cl$_4$–(MBdpa)$_2$}$_n$]** in the interface region between the two solutions. These crystals were used for X-ray structural analysis. Anal. Calcd for $C_{30}H_{36}Cl_4Cu_2N_6 \cdot 2H_2O$: C, 45.87; H, 5.13; N, 10.70; Cl, 18.05%. Found: C, 45.95; H, 5.04; N, 10.20; Cl, 17.48%.

To a methanol solution (0.5 mL) of $CuCl_2$ (2.65 mg, 0.02 mmol) was added a methanol solution (0.5 mL) of **(MBdpa)$_2$** (4.8 mg, 0.010 mmol), and the reaction solution was stirred at 20 °C for 12 h to give a greenish precipitate. The precipitate was washed with methanol and dried under vacuum to give **[{Cu$_2$Cl$_4$–(MBdpa)$_2$}$_n$]** (4.5 mg, 59%) as a green powder. Anal. Calcd for $C_{30}H_{36}Cl_4Cu_2N_6 \cdot 2H_2O$: C, 45.87; H, 5.13; N, 10.70; Cl, 18.05%. Found: C, 45.61; H, 4.70; N, 10.38; Cl, 18.49%.

Apparatus. NMR spectra were recorded on JEOL EX-400 and GX-500 spectrometers. Elemental analysis was carried out by using LECO CHNS-932 and Yanaco MT-5 analysers. UV–vis and photoluminescence spectra were obtained by Shimadzu UV–vis 3100PC and Hitachi F4010 and F4100 spectrometers, respectively. Phosphorescence lifetime was determined by using the Hitachi F4100 spectrophotometer at 20 °C. CD spectra were recorded on a JASCO J-820 spectrofluorometer. MS analysis was performed with JEOL JMS-700 by using 3-nitorobenzylalcohol as a matrix. ESR measurement was carried out with a JEOL JES-RE3X spectrometer in the X-band at 123 K.

Crystal Structure Determination. The crystal structure of **[{Cu$_2$Cl$_4$–(MBdpa)$_2$}$_n$]** was determined at 100 K and 85 K. The diffraction intensity measurement at 100 K was carried out on a Rigaku Saturn CCD area detector system, and the diffraction data at 85 K were measured using a Rigaku R-AXIS RAPID imaging plate diffractometer, both with graphite monochromatized Mo Kα radiation. Selected experimental parameters and crystal data are summarized in Table 1. Diffraction intensity data were corrected for Lorentz and polarization effects. Absorption correction was applied for the dataset at 100 K but not for that at 85 K. The structures were solved by the direct method, using SIR92[37] for the data at 100 K and SHELXS97[38] for those at 85 K. The hydrogen atoms were introduced using the riding model. Both structures were refined by the full-matrix least squares using SHELXL97.[38] All the non-hydrogen atoms were refined anisotropically for the data at 100 K, while only Cu and Cl atoms were refined anisotropically for the data at 85 K.

Results and Discussion

Synthesis of Oligomers of *N*-(*S*)-2-Methylbutyldipyridylamine, (MBdpa)$_m$. *N*-(*S*)-2-Methylbutyldipyridylamine, **MBdpa**, was prepared by NaH promoted deprotonation of

Table 1. Crystal Data and Experimental Conditions

Empirical formula	$C_{30}H_{36}Cl_4Cu_2N_6$	
Formula weight	749.56	
T/K	100(2)	85(2)
Crystal system	monoclinic	monoclinic
Space group	$C2$ (no. 5)	$C2$ (no. 5)
a/Å	18.036(6)	33.558(3)
b/Å	11.674(2)	23.021(2)
c/Å	16.665(5)	19.040(2)
β/°	113.641(10)	119.07(3)
V/Å^3	3214(2)	12857(2)
Z	4	16
μ(Mo Kα)/mm^{-1}	1.687	1.687
Number of measured reflections	16943	25681
Number of independent reflections	7172	19684
R_{int}	0.0583	0.0460
$R1(F_o)$[a] $[F_o^2 > 2\sigma(F_o^2)]$	0.0575	0.0762
$wR2(F_o^2)$[b] [all data]	0.1730	0.3156

a) $R1 = \Sigma||F_o| - |F_c||/\Sigma|F_o|$. b) $wR2 = [\Sigma w(F_o^2 - F_c^2)^2/\Sigma w(F_o^2)^2]^{1/2}$. $w = 1/[\sigma^2(F_o^2) + (0.0673P)^2 + (30.7765P)]$, where $P = (F_o^2 + 2F_c^2)/3$. $w = 1/[\sigma^2(F_o^2) + (0.1532P)^2]$, where $P = (F_o^2 + 2F_c^2)/3$.

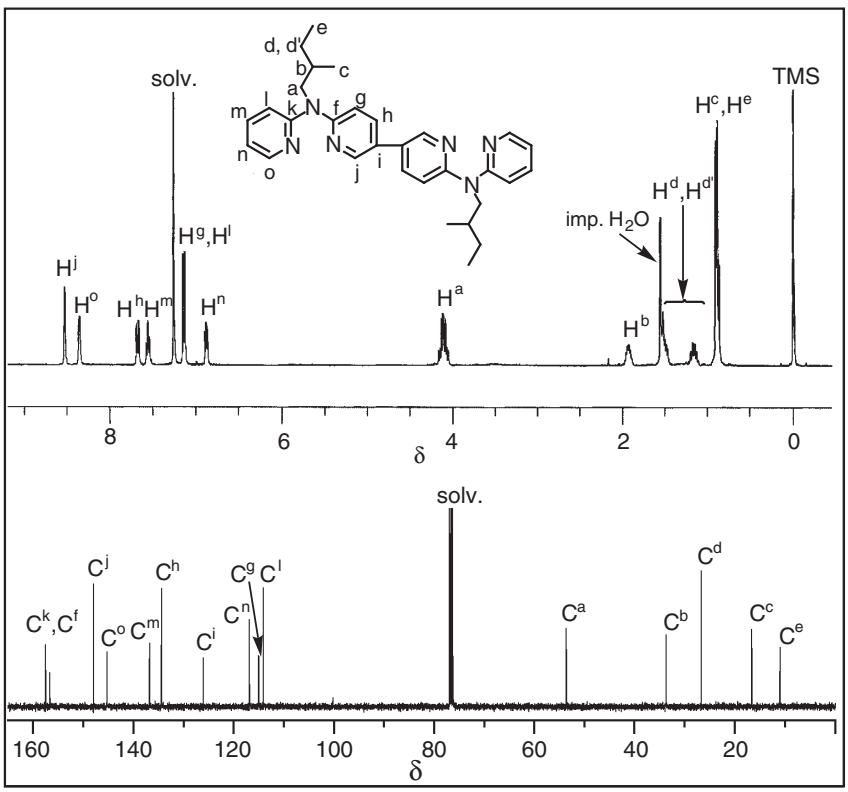

Fig. 1. ^{1}H and ^{13}C NMR spectra of **(MBdpa)$_2$** in $CDCl_3$.

NH group of dpa and following alkylation with (*S*)-1-iode-2-methylbutane. Dimer, trimer, and tetramer of **MBdpa**, **(MBdpa)$_m$** (m = 2, 3, and 4), were synthesized by using organometallic coupling reactions, as shown in Scheme 1.

Figure 1 depicts ^{1}H and ^{13}C NMR spectra of **(MBdpa)$_2$**. The NCH_2 hydrogens (H^a in Fig. 1) and the hydrogen at the chiral center (H^b) give peaks at δ 4.12 and 1.93, respectively. A peak assigned to the two methyl groups (H^c and H^e) is observed at δ 0.89. Methylene hydrogens (H^d and $H^{d'}$) adjacent to the chiral center are diastereotropic each other and show peaks at δ 1.15 and 1.50 in an equal intensity. Peaks due to hydrogens of the pyridine rings are observed in the range of δ 6.85 to 8.53 (see Experimental Section). ^{13}C NMR signals assigned to aromatic and aliphatic carbons of **(MBdpa)$_2$** appear in ranges of δ 114.4–157.8 and of δ 11.4–54.0, respectively, and assignments of these signals are shown in Fig. 1. The assignments were confirmed by using ^{1}H–^{1}H COSY and ^{1}H–^{13}C COSY techniques.

Structures of **(MBdpa)$_3$** and **(MBdpa)$_4$** were also confirmed similarly, by elemental analysis and ^{1}H and ^{13}C NMR and MS spectroscopy.

Cu Complex of (MBdpa)$_2$. Reaction of $CuCl_2$ and **(MBdpa)$_2$** in methanol under stirring conditions gave a powdery copper complex of **(MBdpa)$_2$**. The complex had a composition of **Cu_2Cl_4–(MBdpa)$_2$**, as judged from elemental analytical data; however it was insoluble in organic solvents, which prevented recrystallization of the copper complex.

Single crystals of **[{Cu_2Cl_4–(MBdpa)$_2$}$_n$]** were fortunately obtained in an interface region formed between a methanol solution of $CuCl_2$ and a methanol solution of **(MBdpa)$_2$** formed in an NMR tube. The obtained crystal was also sparingly soluble in the organic solvents, however, it was suited to X-ray crystallographic analysis.

Structure of [{Cu_2Cl_4–(MBdpa)$_2$}$_n$]. Figure 2 illustrates the crystal structure of **[{Cu_2Cl_4–(MBdpa)$_2$}$_n$]** at 100 K. Crystal data and relevant experimental parameters used in the structure determination of **[{Cu_2Cl_4–(MBdpa)$_2$}$_n$]** at 100 K and 85 K are shown in Table 1. Selected bond lengths and angles for **[{Cu_2Cl_4–(MBdpa)$_2$}$_n$]** are listed in Table 2. An asymmetric unit of **[{Cu_2Cl_4–(MBdpa)$_2$}$_n$]** at 100 K contains two **MBdpa** units and two Cu and four Cl atoms. The two **MBdpa** subunits are referred to as A and B. The atoms are labeled with a number that is consistently assigned for the two subunits; the suffix A or B indicates the subunit name. The Cu and Cl atoms are similarly labeled. When we refer to the features common for the two subunits in the following discussion, we use the labels without the suffices for the subunits.

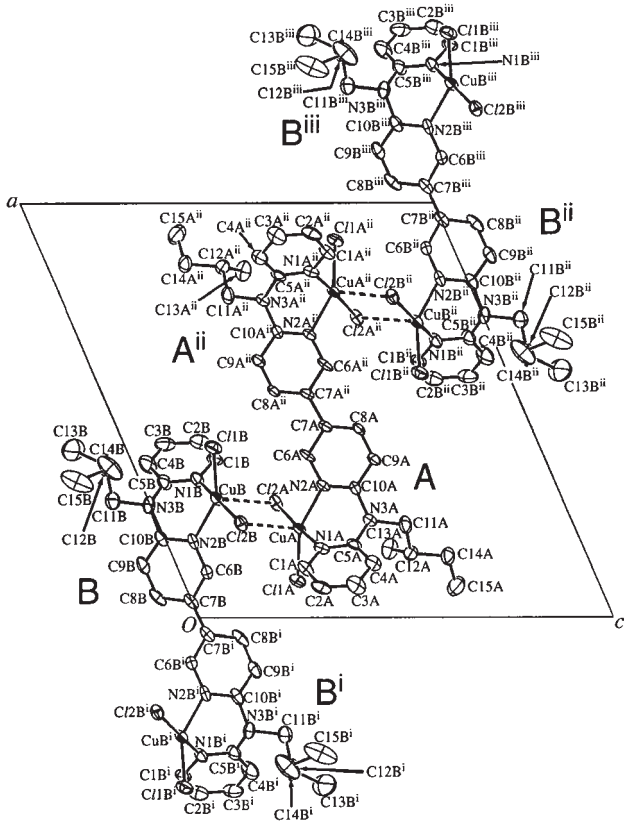

Fig. 2. Structure of **[{Cu_2Cl_4–(MBdpa)$_2$}$_n$]** at 100 K viewed down the *b* axis. Letters A and B represent the subunit names. Symmetry codes: (i) $-x$, y, $-z$; (ii) $1-x$, y, $1-z$; (iii) $1+x$, y, $1+z$.

The two independent **MBdpa** moieties exhibit different conformations for the MB groups: *trans* for the ethyl group and *gauche* for the methyl group in the subunit A and *gauche* for the ethyl group and *trans* for the methyl group in the subunit B. The C7 atom of the **MBdpa** moiety is located close to the twofold axis and bonded to its symmetry equivalent, completing the **(MBdpa)$_2$** molecule. Each **MBdpa** moiety chelates to a Cu atom using its two N atoms (N1 and N2) of the pyridine rings as the donor atoms, while the amine-N atom (N3) does not bind to the Cu atom. The coordination geometry of these **MBdpa** moieties is similar to that found for the 2,2′-dipyridyl(*N*-propenyl)amine (Prdpa) ligand in Cu(Prdpa)$(NO_3)_2$, Zn(Prdpa)$(NO_3)_2$, and Cu(Prdpa)$_2(NO_3)_2$.[32] Two Cl atoms bind to the Cu atom, Cl1 at 2.249(3)–2.254(3) Å and Cl2 at 2.291(3)–2.296(3) Å from Cu, thus completing the neutral **[{Cu_2Cl_4–(MBdpa)$_2$}$_n$]** complexes. The coordination geometry around the Cu atom is distorted square pyramidal (with the geometric parameter τ of 0.39[38]), with N1, N2, Cl1, and Cl2 in the basal square with the *cis* configuration. The Cl2 atom of an adjacent **Cu_2Cl_4–(MBdpa)$_2$** complex is located at 2.629(3)–2.653(3) Å from the Cu center, to occupy the apical site, completing the square pyramidal five coordination. This intermolecular interaction links the **Cu_2Cl_4–(MBdpa)$_2$** complexes into one-dimensional coordination polymer extended along the $a+c$ direction. In other words, the ClCu(μ-Cl)$_2$CuCl cores are concatenated by the **(MBdpa)$_2$** ligands. The Cu···Cu distance in the ClCu(μ-Cl)$_2$CuCl core is 3.619(1) Å. With respect to the midpoint of the two Cu atoms, the ClCu(μ-Cl)$_2$CuCl core and the dpa moieties of the **MBdpa** ligands are approximately symmetric, leading to the opposite chirality for the amine-N atoms (N3A and N3B). Thus the two independent **(MBdpa)$_2$** molecules may be described as a pair of diastereomers that exhibit the same chirality at the MB groups and the opposite chirality at the amine-N atoms.

To obtain diffraction data at lower temperature, we exposed a separate crystal to X-ray irradiation. Preliminary diffraction images taken at room temperature were successfully indexed with the same lattice parameters as that obtained at 100 K. However, upon lowering the temperature to 85 K, there appeared additional diffraction spots that could not be indexed with the unit cell obtained at 100 K. A satisfactory indexing could only be achieved when one assumed a quadrupled unit cell. When the crystal was brought up to room temperature again, the diffraction spots due to the quadrupled cell disappeared, suggesting that the structure of the crystal changed back to that of the higher temperature phase. Since both the phases have the same space group *C*2, the volume of the asymmetric unit is also quadrupled. An asymmetric unit now accommodates eight independent **MBdpa** subunits (named here as A to H). The subunits A, C, E, and G correspond to the subunit A of the 100 K phase and the subunits B, D, F, and H correspond to the subunit B of the 100 K phase. The subunits A, B, C, and D bind to their respective symmetry equivalent counterparts to complete **(MBdpa)$_2$** molecules. The subunits A and B are linked into one coordination polymer and the subunits C and D into another. On the other hand, the subunits E and G complete a **(MBdpa)$_2$** molecule, and F and H another.

Table 2. Selected Interatomic Distances (Å) and Torsion Angles (°) in **[{Cu_2Cl_4–(MBdpa)$_2$}$_n$]**

100 K			
CuA–CuB	3.6193(12)	CuA–N1A	2.025(9)
CuA–N2A	2.036(7)	CuA–Cl1A	2.254(3)
CuA–Cl2A	2.296(3)	CuA–Cl2B	2.629(3)
CuB–N1B	2.019(9)	CuB–N2B	2.024(8)
CuB–Cl1B	2.249(3)	CuB–Cl2B	2.291(3)
CuB–Cl2A	2.653(3)		
N3A–C11A–C12A–C14A	−178.5(9)	N3A–C11A–C12A–C13A	56.2(12)
N3B–C11B–C12B–C14B	−85.9(12)	N3B–C11B–C12B–C13B	142.7(11)
85 K			
CuA–CuB	3.638(4)	CuC–CuD	3.627(3)
CuE–CuF	3.633(4)	CuG–CuH[iv)]	3.619(4)
CuA–N1A	2.019(14)	CuA–N2A	2.046(14)
CuA–Cl1A	2.266(5)	CuA–Cl2A	2.309(5)
CuA–Cl2B	2.636(5)	CuB–N1B	1.996(16)
CuB–N2B	2.056(14)	CuB–Cl1B	2.248(6)
CuB–Cl2B	2.304(5)	CuB–Cl2A	2.647(5)
CuC–N1C	2.018(11)	CuC–N2C	2.039(9)
CuC–Cl1C	2.268(4)	CuC–Cl2C	2.299(4)
CuC–Cl2D	2.601(4)	CuD–N1D	1.952(12)
CuD–N2D	2.060(11)	CuD–Cl1D	2.248(5)
CuD–Cl2D	2.301(5)	CuD–Cl2C	2.640(4)
CuE–N2E	2.058(12)	CuE–N1E	2.061(14)
CuE–Cl1E	2.262(5)	CuE–Cl2E	2.301(5)
CuE–Cl2F	2.629(5)	CuF–N1F	2.021(14)
CuF–N2F	2.054(14)	CuF–Cl1F	2.260(5)
CuF–Cl2F	2.299(5)	CuF–Cl2E	2.637(5)
CuG–N2G	2.034(12)	CuG–N1G	2.054(15)
CuG–Cl1G	2.254(5)	CuG–Cl2G	2.301(5)
CuG–Cl2H[iv)]	2.612(5)	CuH–N1H	1.967(15)
CuH–N2H	2.039(14)	CuH–Cl1H	2.242(5)
CuH–Cl2H	2.300(5)	CuH–Cl2G[v)]	2.645(5)
N3A–C11A–C12A–C14A	−174.8(14)	N3A–C11A–C12A–C13A	60.8(18)
N3B–C11B–C12B–C14B	−82(2)	N3B–C11B–C12B–C13B	146(2)
N3C–C11C–C12C–C14C	−175.9(14)	N3C–C11C–C12C–C13C	57.1(19)
N3D–C11D–C12D–C14D	−81(2)	N3D–C11D–C12D–C13D	146(2)
N3E–C11E–C12E–C14E	−179.7(14)	N3E–C11E–C12E–C13E	56.8(18)
N3F–C11F–C12F–C14F	−83.3(15)	N3F–C11F–C12F–C13F	146.1(13)
N3G–C11G–C12G–C14G	−177.6(14)	N3G–C11G–C12G–C13G	57.7(17)
N3H–C11H–C12H–C14H	97(2)	N3H–C11H–C12H–C13H	−40(2)

Symmetry codes: (iv) $x, y, z-1$; (v) $x, y, z+1$.

These four subunits are linked into one coordination polymer. The structures of the subunits A–H viewed down the *b* axis are depicted in two separate illustrations for clarity. Figure 3 depicts the coordination polymer consisting of the subunits D, E, F, and G that are located around $y \approx 1/4$. The subunits A, C, E, and G roughly retain the conformation of subunit A at 100 K and the conformation of the subunits B, D, and F are similar to that of subunit B at 100 K. However, the MB group of subunit H exhibits a different conformation from others, which characterizes the structure at 85 K. As depicted in Fig. 2, the MB group of subunit B of the 100 K phase exhibits larger displacement parameters than that of subunit A, which may be attributed to the contribution of the conformer that has the same structure as subunit H of the 85 K phase. The 100 K phase presumably contains this conformer as a disorder component. Therefore, we conclude that the cell quadrupling observed at 85 K is due to the ordering of the MB groups in the subunits B, D, F, and H. This ordering is associated with the rearrangement of the coordination polymer chains. The matrix associated with the cell quadrupling transforms the lattice constant at 100 K to $a_T = 33.332$ Å, $b_T = 23.348$ Å, $c_T = 19.026$ Å, and $\beta_T = 119.72°$ (suffix T denotes transformed values). Comparison of these values with the lattice constants at 85 K indicates that the repeat distance along the coordination polymer, which is parallel to the direction of c_{85K} (or $a_{100K} + c_{100K}$), does not change upon the phase transition. On the other hand, a_T is shorter than a_{85K} and b_T is shorter than b_{85K} by about 0.2–0.3 Å, indicating that the spacing between the coordination polymers has changed. The chains consisting of the subunits A + B and C + D, which were equivalent and thus had the same *y* coordinates in the 100 K phase, are displaced from each other along the *b* direction with 0.153 Å in

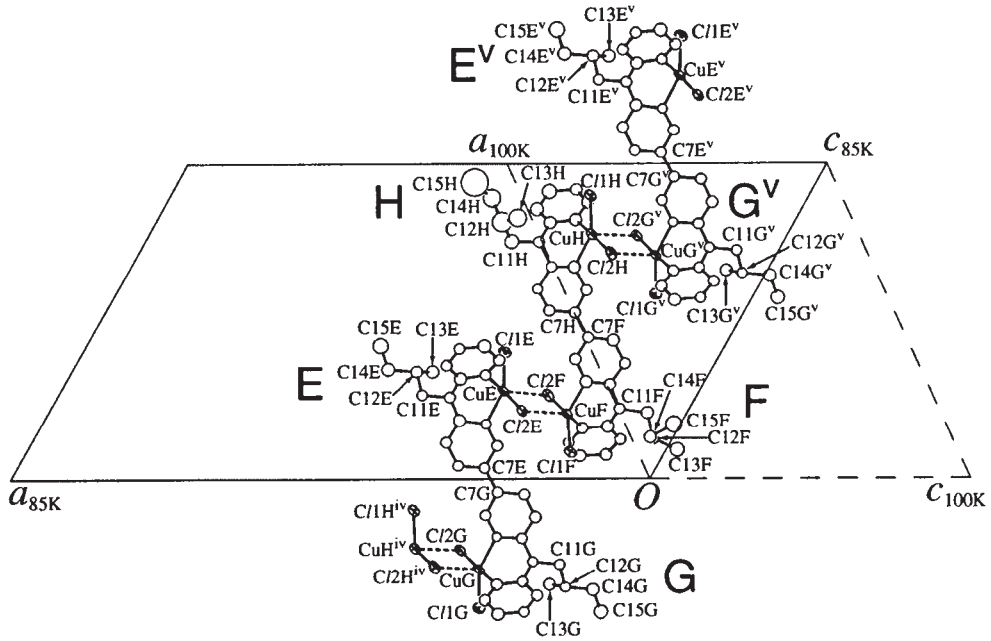

Fig. 3. Structure of the subunits E, F, G, and H of the 85 K phase. Only selected atoms are labeled for clarity. Cell outline for the 100 K phase is also drawn to illustrate the relationship between the phases. Note that the conformation of C11–C15 in the subunit H is different form those in the subunits B, D, and F (and the subunit B of the 100 K phase). Symmetry codes: (iv) $x, y, z-1$; (v) $x, y, z+1$.

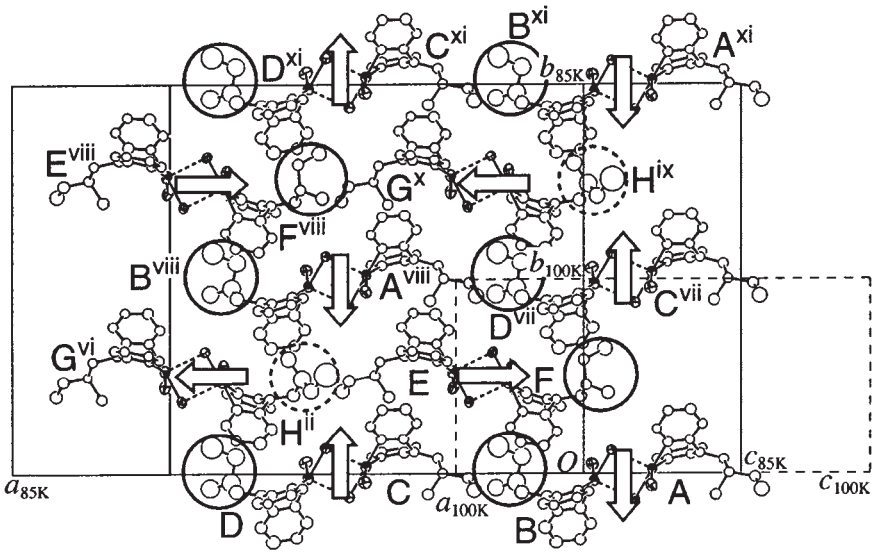

Fig. 4. Packing diagram of **[{Cu$_2$Cl$_4$–(MBdpa)$_2$}$_n$]** at 85 K projected down to the *ab* plane. Only a half of the unit cell ($0 < z < 1/2$) is shown for clarity. The MB groups of the subunits B, D, and F are surrounded by circles with solid lines and H with broken lines. Arrows indicate the dislocations of the coordination polymers. Symmetry codes: (ii) $1-x, y, 1-z$; (vi) $1-x, y, -z$; (vii) $-1/2+x, 1/2+y, z$; (viii) $1/2+x, 1/2+y, z$; (ix) $1/2-x, 1/2+y, 1-z$; (x) $1/2-x, 1/2+y, -z$; (xi) $x, y, 1+z$.

the 85 K phase (the displacement was calculated based on the midpoints of the two Cu atoms). The chain consisting of the subunits D + E + F + G at $x \approx 1/4$ and $y \approx 3/4$ is shifted along the *a* direction with 0.184 Å from that at $x \approx 1/4$ and $y \approx 1/4$ (they had the same *x* coordinates in the 100 K phase). As shown in Fig. 4, these dislocations lead to the different shapes of the cavities that accommodate the MB groups of subunits F and H, which then lead to the different conformations.

UV–Vis Data of (MBdpa)$_m$ and the Cu–(MBdpa)$_m$ Complex. The UV–vis and photoluminescence (PL) data of **(MBdpa)$_m$** are summarized in Table 3. The absorption peak due to a π–π^* transition of **(MBdpa)$_m$** shifts to a longer wavelength with increase in the chain length, indicating that the electronic system of **MBdpa** is expanded even through the C–N–C non-conjugating bond in **(MBdpa)$_m$**.

Optical data of **[{Cu$_2$Cl$_4$–(MBdpa)$_2$}$_n$]** could not be obtained due to its poor solubility in organic solvents; however,

Table 3. UV–Vis and PL Data of **(MBdpa)$_m$**

	Absorption in $CHCl_3$/nm (Molar coefficient/mol^{-1} L cm^{-1})	Photoluminescence in THF (Φ[a], %)	EX[b]
(MBdpa)$_2$	350 (52000)	389 (63)	345
(MBdpa)$_3$	365 (53000)	404 (67)	365
(MBdpa)$_4$	369 (78000)	409 (76)	368

a) Quantum yield of the photoluminescence ($\Phi_f + \Phi_p$). b) Peak position of the excitation monitored at the photoluminescence peak.

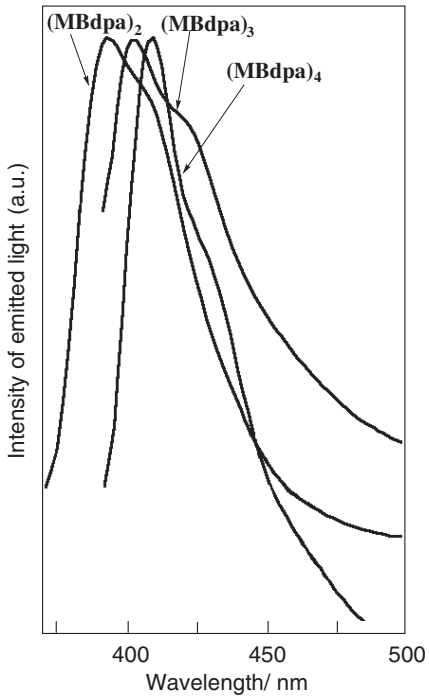

Fig. 5. Photoluminescence spectra of **(MBdpa)$_m$** in THF.

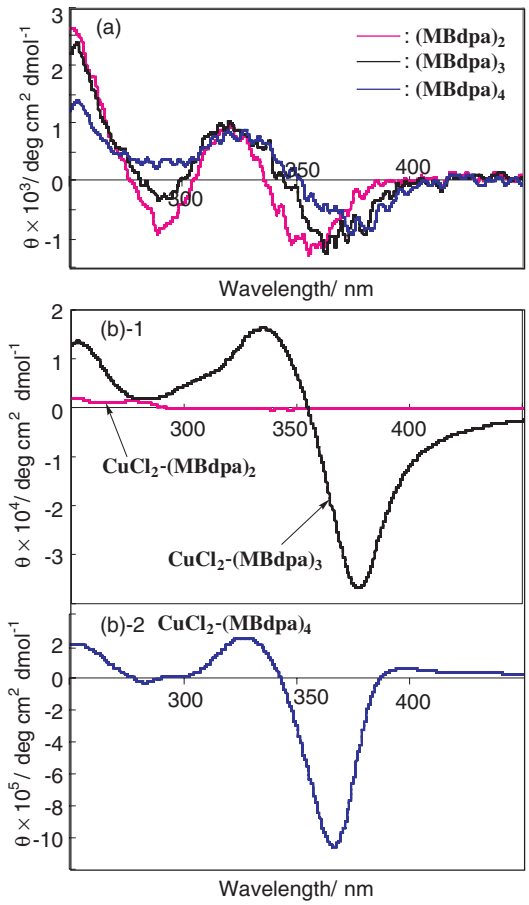

Fig. 6. Circular dichroic spectra of (a) **(MBdpa)$_m$** in CH_3CN and (b) CH_3CN solutions of a *m*:1 mixture of $CuCl_2$ and **(MBdpa)$_m$** ($m = 2$ and 3 for (b)-1 and 4 for (b)-2, respectively). Concentration of **(MBdpa)$_m$** is 0.60×10^{-3} M (molarity is based on the **MBdpa** unit).

UV–vis, photoluminescence, and circular dichromism (CD) measurements of the CH_3CN solution of **(MBdpa)$_2$** in the presence of a CH_3CN solution of $CuCl_2$ were carried out. Addition of the CH_3CN solution of $CuCl_2$ into the CH_3CN solution of **(MBdpa)$_2$** caused a shift of the absorption peak by 15 nm to a shorter wavelength. The hypsochromic shift seems to be attributed to reduction of electronic interaction between the two **MBdpa** units of **(MBdpa)$_2$** due to the copper complexation, which seems to decrease the angle of C(2-position of the pyridine ring)–N–C(2′-position of the pyridine ring).

Photoluminescence Data. It has been reported that dpa exhibits a fluorescence peak at 340 nm and a phosphorescence peak at 410 nm in solutions when irradiated with a 284 nm light corresponding to a ^1L_a band ($^1S_1$–$^1S_0$ transition).[33] The **(MBdpa)$_m$** oligomers ($m = 2$, 3, and 4) give also photoluminescence spectra as depicted in Fig. 5. Each of the photoluminescence spectra show a maximum peak and a shoulder peak. The shoulder peak was ascribed to the phosphorescence of **(MBdpa)$_m$** based on its lifetime. The phosphorescence lifetime of **(MBdpa)$_2$** and **(MBdpa)$_3$** obtained for the shoulder peak, 689 ms and 682 ms, respectively, were somewhat shorter than that of dpa (1.1 s[33]). It has been reported that the phosphorescence lifetime of π-conjugated macromolecules becomes shorter as the π-conjugation length increases.[39] Total quantum yields $\Phi_p + \Phi_f$ of **(MBdpa)$_m$** somewhat increased with increase in the chain length, as shown in Table 3.

Addition of $CuCl_2$ into the CH_3CN solution of **(MBdpa)$_m$** caused decrease of intensity of the PL, probably due to the existence of the chloride ligands, which are known to quench PL through heavy atom effects. A similar quenching effect of metal complexation on PL of derivatives of dpa has been reported.[34]

Circular Dichromism (CD). Figure 6 depicts circular dichroic spectra of CH_3CN solutions of **(MBdpa)$_m$** ($m = 2$, 3, and 4) and a mixture of $CuCl_2$ and **(MBdpa)$_m$** in a *m*:1 molar

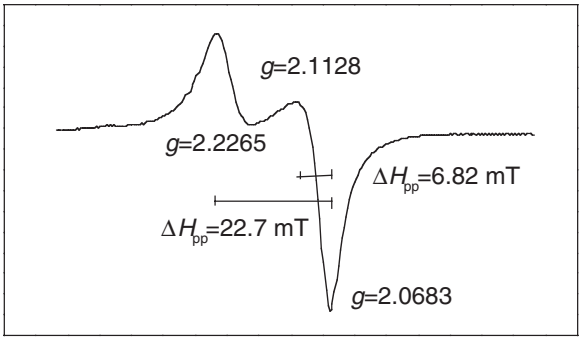

Fig. 7. ESR spectrum of **[{Cu_2Cl_4–(MBdpa)$_2$}$_n$]** at 123 K.

ratio. **(MBdpa)$_m$** showed CD signal with Cotton effect with a similar intensity in the range of 180 nm to 380 nm (Fig. 6a). The wavelength of the Cotton effect around 350 nm corresponds to the position of the UV–vis peak. The CH_3CN solutions made of $CuCl_2$ and **(MBdpa)$_m$** ($m = 3$ and 4) showed CD signals at positions similar to those of **(MBdpa)$_m$** ($m = 3$ and 4) with a higher θ value, compared with **(MBdpa)$_m$** ($m = 3$ and 4) themselves. As judged from these data, **(MBdpa)$_m$** ($m = 3$ and 4) may form helical structures by the complexation with Cu^{2+}. A solution of $CuCl_2$ with **(MBdpa)$_2$**, to the contrary, did not show any CD signal in the range of 280–450 nm. As discussed above, single crystal X-ray analysis revealed that **[{Cu_2Cl_4–(MBdpa)$_2$}$_n$]** had a polymeric structure containing no helical conformation. The **Cu–(MBdpa)$_2$** complex dissolved in the solution seems to have a similar structure.

ESR Spectrum. Figure 7 depicts the ESR spectrum of **[{Cu_2Cl_4–(MBdpa)$_2$}$_n$]**. Two types of g values, $g_\perp$ and $g_\parallel$, have been used to distinguish unambiguously between $d_{x^2-y^2}$ and d_{z^2} ground states for which $g_\parallel > g_\perp$ and $g_\perp > g_\parallel$, respectively.[40,41] The ESR spectrum shows three signals ($g = 2.227$, 2.113, and 2.068), and no hyperfine structure is observed. These g-values can be classified as $g_\perp = 2.09$ and $g_\parallel = 2.227$, confirming that the unpaired electron largely resides in the copper(II) $d_{x^2-y^2}$ orbital.

Conclusion

Dipyridylamine oligomers having *N*-(*S*)-2-methylbutyl side chains, **(MBdpa)$_m$**, were obtained by the organometallic coupling reactions. Copper complexation of **(MBdpa)$_2$** provided a new coordination polymer, **[{Cu_2Cl_4–(MBdpa)$_2$}$_n$]**. Single crystal X-ray analysis revealed that **[{Cu_2Cl_4–(MBdpa)$_2$}$_n$]** underwent the phase transition between 100 and 85 K in the solid state, resulting in a quadrupling of the unit cell at the lower temperature. UV–vis data indicated that **(MBdpa)$_m$** had an expanded electron system along the oligomer main chain. **(MBdpa)$_m$** showed photoluminescence (PL) in THF and their phosphorescence component was revealed by the time resolved PL. ESR data showed that the magnetic orbital of **[{Cu_2Cl_4–(MBdpa)$_2$}$_n$]** was formed mainly by the $d_{x^2-y^2}$ orbital.

The authors gratefully acknowledge Dr. Y. Nishihara and Dr. M. Horie in our institute for X-ray measurements at 100 K. This research was partly supported by 21st Century COE program.

References

1 S. R. Batten and R. Robson, *Angew. Chem., Int. Ed.*, **37**, 1460 (1998).
2 M. Fujita, *Chem. Soc. Rev.*, **27**, 417 (1998).
3 A. J. Blake, N. R. Champness, P. Hubberstey, W.-S. Li, M. A. Withersby, and M. Schröder, *Coord. Chem. Rev.*, **183**, 117 (1999).
4 P. J. Hagrman, D. Hagrman, and J. Zubieta, *Angew. Chem., Int. Ed.*, **38**, 2638 (1999).
5 R. P. Kingsborough and T. M. Swager, *Progr. Inorg. Chem.*, **48**, 123 (1999).
6 M. Eddaoudi, D. B. Moler, H. Li, B. Chen, T. M. Reineke, M. O'Keeffe, and O. M. Yaghi, *Acc. Chem. Res.*, **31**, 319 (2001).
7 S. R. Batten, *Curr. Opin. Solid State Mater. Sci.*, **5**, 107 (2001).
8 B. Moulton and M. J. Zaworotko, *Chem. Rev.*, **101**, 1629 (2001).
9 R. Song, K. M. Kim, and Y. S. Sohn, *Inorg. Chem.*, **42**, 821 (2003).
10 C. Näther, M. Wriedt, and I. Jess, *Inorg. Chem.*, **42**, 2391 (2003).
11 B. Abrahams, S. R. Batten, B. F. Hoskins, and R. Robson, *Inorg. Chem.*, **42**, 2654 (2003).
12 C. Näther and I. Jess, *Inorg. Chem.*, **42**, 2968 (2003).
13 C.-L. Chen, C.-Y. Su, Y.-P. Cai, H.-X. Zhang, A.-W. Xu, B.-S. Kang, and H.-C. zur Loye, *Inorg. Chem.*, **42**, 3738 (2003).
14 Y. Cui, H. L. Ngo, P. S. White, and W. Lin, *Chem. Commun.*, **2003**, 994.
15 R. Horikoshi, T. Mochida, and H. Moriyama, *Inorg. Chem.*, **41**, 3017 (2002).
16 J. A. Barron, S. Glazier, S. Bemhard, K. Takada, P. L. Houston, and H. D. Abruña, *Inorg. Chem.*, **42**, 1448 (2003).
17 J.-M. Lehn, A. Rigault, J. Siegel, J. Harrowfield, B. Chevrier, and D. Moras, *Proc. Natl. Acad. Sci. U.S.A.*, **84**, 2565 (1987).
18 F. A. Cotton, L. M. Daniels, G. T. Jordan, IV, and C. A. Murillo, *Polyhedron*, **17**, 589 (1998).
19 Report on Fe complex: C. D. Burbridge and D. M. L. Goodgame, *J. Chem. Soc. A*, **1967**, 694.
20 J. C. Bailar, Jr and S. Kirschner, *Inorg. Synth.*, **5**, 184 (1957).
21 D. M. L. Goodgame, *J. Chem. Soc. A*, **1966**, 63.
22 F. A. Cotton, L. M. Daniels, G. T. Jordan, IV, and C. A. Murillo, *J. Am. Chem. Soc.*, **119**, 10377 (1997).
23 R. Clérac, F. A. Cotton, K. R. Dunbar, T. Lu, C. A. Murillo, and X. Wang, *J. Am. Chem. Soc.*, **122**, 2272 (2000).
24 R. Clérac, F. A. Cotton, L. M. Daniels, K. R. Dunbar, K. Kirschbaum, C. A. Murillo, A. A. Pinkerton, A. J. Schultz, and X. Wang, *J. Am. Chem. Soc.*, **122**, 6226 (2000).
25 R. Clérac, F. A. Cotton, L. M. Daniels, K. R. Dunbar, C. A. Murillo, and X. Wang, *Inorg. Chem.*, **40**, 1256 (2001).
26 T. J. Hurley and M. A. Robinson, *Inorg. Chem.*, **7**, 33 (1968).
27 C. D. Burbridge and D. M. L. Goodgame, *J. Chem. Soc. A*, **1968**, 237.
28 S. Aduldecha and B. Hathway, *J. Chem. Soc., Dalton Trans.*, **1991**, 993.
29 J. E. Johnson, R. A. Jacobson, and T. A. Beineke, *J. Chem. Soc. A*, **1971**, 1371.
30 L.-P. Wu, P. Field, T. Morrissey, C. Murphy, P. Nagle, B. Hathaway, C. Simmons, and P. Thornton, *J. Chem. Soc.,*

Dalton Trans., **1990**, 3835.

31 G. J. Pyrka, M. El-Mekki, and A. A. Pinkerton, *J. Chem. Soc., Chem. Commun.*, **1991**, 84.

32 T. D. Coombs, B. J. Brisdon, C. P. Curtis, M. F. Mahon, S. A. Brewer, and C. R. Willis, *Polyhedron*, **20**, 2935 (2001).

33 P. Jana, T. Ganguly, S. K. Sarkar, A. Mitra, and P. K. Mallick, *J. Photochem. Photobiol., A*, **94**, 113 (1996).

34 C. Seward, J. Pang, and S. Wang, *Eur. J. Inorg. Chem.*, **2002**, 1390.

35 W.-L. Jia, Q.-D. Liu, D. Song, and S. Wang, *Organometallics*, **22**, 321 (2003).

36 B. von Bogdanovic, M. Kröner, and G. Wilke, *Justus Liebigs Ann. Chem.*, **699**, 1 (1966).

37 A. Altomare, G. Cascarano, C. Giacovazzo, A. Guagliardi, M. C. Burla, G. Polidori, and M. Camalli, *J. Appl. Crystallogr.*, **27**, 435 (1994).

38 G. M. Sheldrick, "SHELX97, Program for the Crystal Structure Analysis," University of Göttingen, Göttingen, Germany (1997).

39 D. Hertel, S. Setayesh, H.-G. Nothofer, U. Scherf, K. Müllen, and H. Bässler, *Adv. Mater.*, **13**, 65 (2001).

40 B. J. Hathaway and A. A. G. Tomlinson, *Coord. Chem. Rev.*, **5**, 1 (1970).

41 S.-Q. Zang, R.-J. Tao, Q.-L. Wang, N.-H. Hu, Y.-X. Cheng, J.-Y. Niu, and D.-Z. Liao, *Inorg. Chem.*, **42**, 761 (2003).